International Journal of Heat and Mass Transfer 140 (2019) 731–742

Contents lists available at ScienceDirect

International Journal of Heat and Mass Transfer

journal homepage: www.elsevier.com/locate/ijhmt

An experimental investigations of the melting of RT44HC inside a horizontal rectangular test cell subject to uniform wall heat flux

Mohamed Fadl *, Philip C. Eames

Centre for Renewable Energy Systems Technology (CREST), Loughborough, United Kingdom University, Loughborough (Leicestershire) LE11 3TU, United Kingdom

ARTICLE INFO

Article history:
Received 25 March 2019
Received in revised form 10 June 2019
Accepted 13 June 2019

Keywords:
PCM
Heat flux
Nusselt number
Heat transfer
Thermal energy storage and melting

ABSTRACT

This study experimentally investigates the effect of different values of wall heat flux intensity on the melting of RT44HC Phase Change Material (PCM) in a rectangular test cell. A new novel experimental test rig to provide accurate data for the validation of numerical models of phase change was developed. The designed and constructed test rig consists of a horizontal rectangular cross-section test cell formed from polycarbonate sheet with copper plates and mica heaters to provide controlled uniform wall heat flux. Experiments were performed for three constant uniform wall heat flux values (q''_{wall} = 675, 960 and 1295 W/m^2) applied to both left and right sides of the test cell. An imaging technique was used to visualize and record the movement of the solid-liquid interface using a Canon EOS DSLR Camera. The results obtained show a strong correlation between the magnitude of wall heat flux which drives the convective heat transfer and melt fraction development in the PCM. The results also show that increasing the input power from 675 W/m^2 to 960 W/m^2 to 1295 W/m^2 reduces the total time for the melting process by 26.3% and 42.10% respectively. The raw data set comprised of measured temperatures and observation of melt fraction development provide a useful data set for validation of numerical models aiming to simulate the melting process in a rectangular cross-section test cell.

1. Introduction

Latent heat thermal energy storage (LHTES) has a wide range of potential engineering applications and has recently gained considerable attention for space heating and cooling due to environmental concerns and the rising cost of fossil fuels. Applications are particularly interesting due to domestic space cooling/heating in extremely hot/cold areas where electrical energy consumption varies greatly during the night and the day [1,2].

LHTES can be used to address the time-of-use mismatch between heat supply and demand. Phase Change Materials (PCMs) have the advantages of high thermal energy storage density, resulting in smaller store size, the potential for near constant temperature of operation can result in improved efficiency when compared to a sensible heat storage system [3]. A large number of non-toxic PCMs are available with melting temperatures covering a wide range of applications. These features make PCMs an attractive option for many applications, for example passive temperature control of buildings, compact thermal energy storage systems, medical applications requiring constant temperature, storage of recovered industrial waste heat for later use and temperature control of electronics [4].

The complex nature of the PCM melting-solidification process and the combined conductive and convective heat transfer processes within the PCM are of continuing interest to researchers. Experimental analysis is required in order to better understand the heat transfer mechanisms and the differences in performance that result for different designs of PCM thermal storage systems. Such experimental analysis will enable system designs to be optimised and suitable applications identified [5].

Experimental and numerical investigations have been performed in recent years with the aim of improving understanding of the heat transfer within the PCM, particularly at the moving solid-liquid interface. This will enable optimum storage system designs to be developed for specific applications, e.g. rectangular enclosures, spherical capsules, tubes or cylinders and annular cavities [5]. Rectangular enclosures are one of the most common geometrical configurations used in LHTES systems. Due to their wide-ranging engineering applications in fields including metallurgy,

* Corresponding author at: Centre for Renewable Energy Systems Technology (CREST), Wolfson School of Mechanical, Electrical and Manufacturing Engineering, Garendon Wing, Holywell Park, Loughborough University, Loughborough, Leicestershire, LE11 3TU, United Kingdom. Tel.: +44 1509 635609.

E-mail addresses: m.s.fadl@lboro.ac.uk (M. Fadl), philip.c.eames@lboro.ac.uk (P.C. Eames).

https://doi.org/10.1016/j.ijheatmasstransfer.2019.06.047
0017-9310/

Nomenclature

A_w	the surface area of the hot wall [m^2]
C	specific heat at constant pressure [kJ/kg K]
f	liquid fraction percentage
H	characteristic length [m]
h_{latent}	latent heat [kJ/kg]
h	heat transfer coefficient [W/m^2 K]
I	electric current [amp]
k	thermal conductivity [W/m K]
L	length of the heating plate [m]
M	mass [kg]
n	number of thermocouples
NP_0	number of pixels with 0 value
NP_t	total number of pixels
Nu	Nusselt number
$Q_{sensible}$	sensible absorbed energy [kJ]
Q_{latent}	total absorbed energy [kJ]
q″	heat flux [W/m^2]
t	time (t)
T	temperature (°C)
T_{m1}	the onset of melting temperature (°C)
T_{m2}	the endset of melting temperature (°C)
T_{mean}	mean temperature (°C)
v	volume [m^3]
V	electric potential [volt]
W	the width of the heating plate [m]

Greek Symbols

β	expansion coefficient [1/K]
μ	dynamic viscosity [kg/ m s]
ρ	density, [kg/m^3]

Subscripts

i	Initial
s	Solid
w	Wall

Abbreviations

PCMs	phase change materials
liq	Liquid
DSLR	digital single-lens reflex

casting and thermal energy storage [6], they have received much attention.

Several recent studies have focused on vertical/horizontal rectangular enclosures with imposed boundary conditions (BC) of a) constant wall temperature (CWT), and (b) constant wall heat flux (CWF) [7] and [8]. This is due to their common occurrence in a range of potential applications, including waste heat recovery systems, solar thermal systems and cooling systems for electronic devices.

Wang Y et al. [9] performed an experimental investigation of the PCM melt process in the vicinity of a uniform temperature heated vertical wall in a rectangular enclosure. From the experiments, it was clear from the variation of Nusselt number with the time that three different heat transfer regimes occurred during the melt process.

El Qarnia H. et al. [10] performed a numerical investigation to predict heat transfer by natural convection during melting of the PCM, n-eicosane contained in a rectangular enclosure acting as a heat sink. In the simulation three heat sources protrude from one of the vertical enclosure walls supplying heat at a uniform constant rate. Simulations show the impact of three key parameters, Rayleigh number, heat source position and enclosure aspect ratio, on the cooling capacity of the PCM based heat sink. The predictions showed that heat from the protruding heat sources is removed in part by natural convection in the liquid PCM while the rest is conducted to the wall before being transferred to the PCM in the enclosure.

Gong et al. [11] simulated free convective melting of a PCM in a rectangular cavity with an isothermally heated vertical wall using the Petrov-Galerkin finite element technique in combination with a fixed grid and a primitive variable formulation. The enthalpy-porosity model was employed to represent the physics at the solid-liquid interface and allow prediction of flow in this region. Predictions showed that inverting the container at an appropriate stage during the melting process was an effective technique to enhance free convection in the phase change material, with a 50% increase in thermal energy charge rate obtained during melting.

Zhao et al. [12] performed a two-dimensional visualization experiment of the close contact melting process of a PCM in a rectangular cavity inclined at different angles (0°,15°,30°,45°, 60°,75°,90°). From the experiments, the shortest total melting time was when the tilt angle was 60°.

Kamkari B et al. [13] investigated experimentally the heat transfer process and melting behaviour during the solid-liquid phase change of lauric acid (Pr = 100) in a rectangular enclosure at different inclination angles (0°,45°,90°). They found that as the inclination angle is decreased from 90° to 0°, the convection currents in the enclosure increase and chaotic flow structures appear. When melting commences in the horizontally inclined enclosure (0°), the solid-liquid interface line becomes wavy which implies the formation of Benard convection cells in the liquid PCM. Finally, the heat transfer enhancement ratio for the horizontal enclosure (0°) is more than two times higher than that of the vertical enclosure(90°).

Huang et al. [14] presented an experimental investigation into the effects of convection and crystalline segregation within a PCM on the heat transfer within different internally finned PCM containers attached to the back of PV panels to provide cooling. The results obtained from the experiments were useful in optimising the design of PV/PCM systems aimed at reducing the rise of PV temperature during operation.

Kamkari and Amlashi [15] investigated numerically the melting of a PCM in both vertical and inclined rectangular enclosures. The predictions show that the heat transfer rate increases and the melting time decreases when the inclination angle of the enclosure is reduced. This was attributed to the intensification of natural convective flow within the PCM.

Emam et al. [16] performed experiments to investigate the melting of three different PCMs (RT25HC, RT35HC, and RT44HC) for three distinct heat flux values, 2000, 2950, 3750 W/m^2 with the aim of providing passive thermal regulation for electronic devices and concentrator photovoltaic (CPV) systems. The experiments revealed that RT35HC PCM achieved a maximum temperature reduction in the operating temperature of electronic components or CPV cells due to its higher absorbed heat per unit volume.

Shatikian et al. [17] performed a numerical parametric investigation into the melting of a PCM in a heat storage unit with vertical internal fins and a horizontal base to which a constant heat flux was applied. The predictions indicate that the transient phase change process depends on a number of system parameters with

the most important being the temperature difference between the base and the mean PCM melt temperature and the thickness and height of the fins.

Kamkari B and Shokouhmand H [18] evaluated experimentally the influence of incorporating horizontal partial fins on the transient melting behaviour of lauric acid (PCM) in a rectangular cavity. The experimental results showed that increasing the number of partial fins reduced the time required to complete the melting phase and improved the total heat transfer rate.

Many researchers have studied the role of natural convection during the melting process in different geometries as mentioned above. There is however no study in the literature that specifically investigates the effect of constant uniform heat flux intensity on opposite vertical walls of a horizontal rectangular test cell on natural convection and melting rates. Wall heat flux is an important parameter which influences the rate of heat transfer and melt front development in many applications and so is the focus of this paper.

Huang et al. [19] experimentally investigated the feasibility of managing the temperature of electronic devices using expanded graphite composite phase change materials. Their experimental results showed that the thermal performance of the composite PCM is dependent on the input power density from the electronic chip, the heat storage density of the composite, the thermal conductivity of the composite, and the thickness of the composite used.

Usman et al. [20] performed an experimental study of PCM based finned (inline and staggered) and un-finned heat sinks for passive cooling of electronics using paraffin wax RT44HC and RT35HC. The results suggested that using triangular shaped inline heat sinks filled with RT44HC provided the best solution for passive thermal management of electronic devices because of its elongated latent heat phase and shortened latent cooling phase, both due to its high latent heat capacity.

In the current study, the melt process of PCM RT44HC inside a horizontal rectangular cross-section test cell has been evaluated experimentally. The test cell was subject to 3 different intensities of uniform wall heat flux applied to both left and right vertical sides, with all other wall conditions essentially adiabatic.

The overall objectives of the proposed study were to (1) visually observe and record the movement of the solid-liquid interface with time, (2) measure the temperature distribution within the PCM with high accuracy and resolution, and (3) to develop an experimental data set (temperature distribution and location of solid-liquid interface) suitable for validation of future simulation work on natural convection inside LHTES of similar geometric design

2. Experimental study

This aim of this research was to investigate experimentally the effect of input wall heat flux intensity on the transient melting process in a horizontal rectangular test cell and measure the transient temperature distribution within the PCM. A horizontal test cell with a rectangular cross-section filled with organic PCM RT44HC which can be subjected to a uniform wall heat flux from both left and right horizontal sides was designed and fabricated.

A schematic of the experimental setup is presented in Fig. 1. It consists of a rectangular cross-section horizontally oriented PCM test cell, insulation, electric mica heaters, data acquisition system, DSLR camera, thermocouples, power supply and voltage transformer.

The rectangular test cell was fabricated from 12 mm thick transparent polycarbonate sheet (Thermal conductivity of 0.2 W/m K) with a maximum operating temperature of 150 °C and density of 1190 kg/m^3 to allow observation of the development of the melt fraction of the RT44HC with time. The interior dimensions of the test cell were 200 mm width, 76 mm height and 176 mm depth as shown in Fig. 2.

Four holes in the upper side of the test cell were drilled and used to introduce the liquid PCM into the store and to provide space for thermal expansion of the liquid PCM that occurs during the melting process. Thin 2 mm copper plates [21] with an area of 100 × 200 mm from the right and left horizontal sides of the test cell on which Mica heating pads are mounted to provide uniform wall heat flux to the plates. The selection of copper plate for the end walls was based on compatibility with the PCM, its long life and high thermal conductivity 401 W/m K. The Mica heater which could operate up to a maximum voltage of 240 VAC was connected to an adjustable AC power supply to allow heat input rate to be varied.

In the experiments, the vertical middle plane of the test cell was chosen to monitor the temperature of the PCM. 21 T-type thermocouples formed from 0.26 mm diameter wire with a calibrated accuracy of ±0.3 °C were placed in seven columns and three rows as shown in Fig. 3. These were connected to a data logger and temperatures were recorded during the melting process.

Three thermocouples distributed on the left and right heating surfaces of the PCM test cell as shown in Fig. 4 measure surface temperature. Two additional thermocouples located outside the test cell were used to measure the ambient and insulation temperatures.

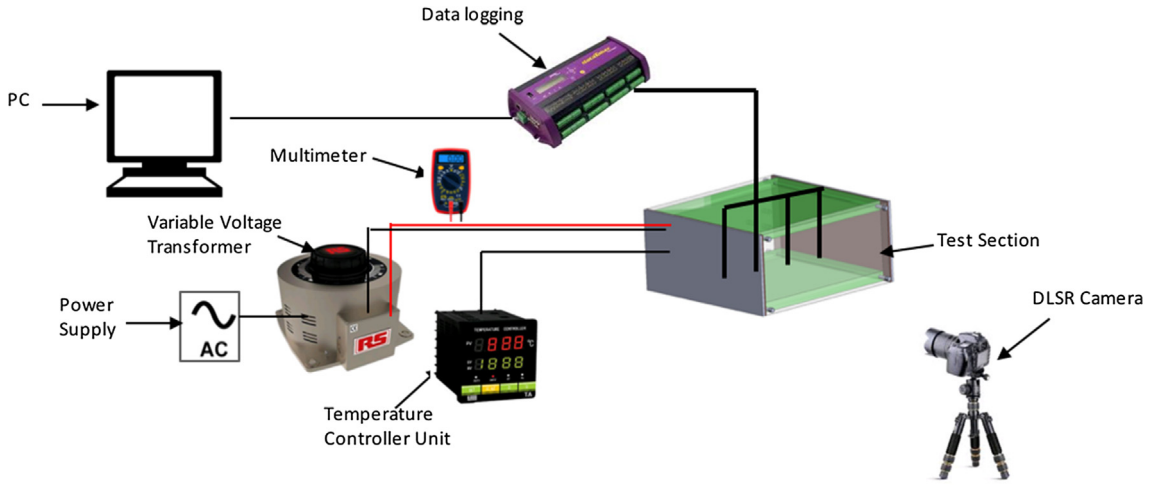

Fig. 1. A schematic diagram of the developed experimental apparatus.

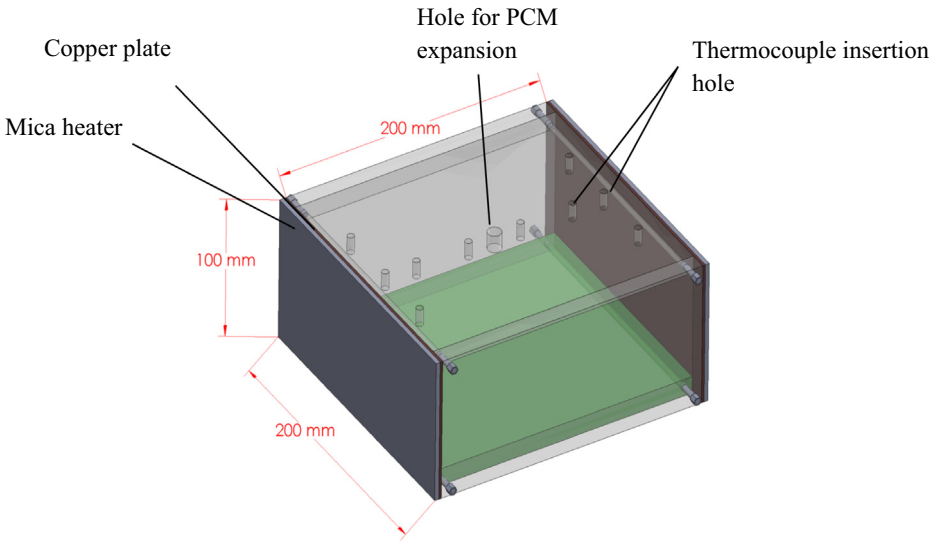

Fig. 2. Schematic diagram of the rectangular cross-section test cell.

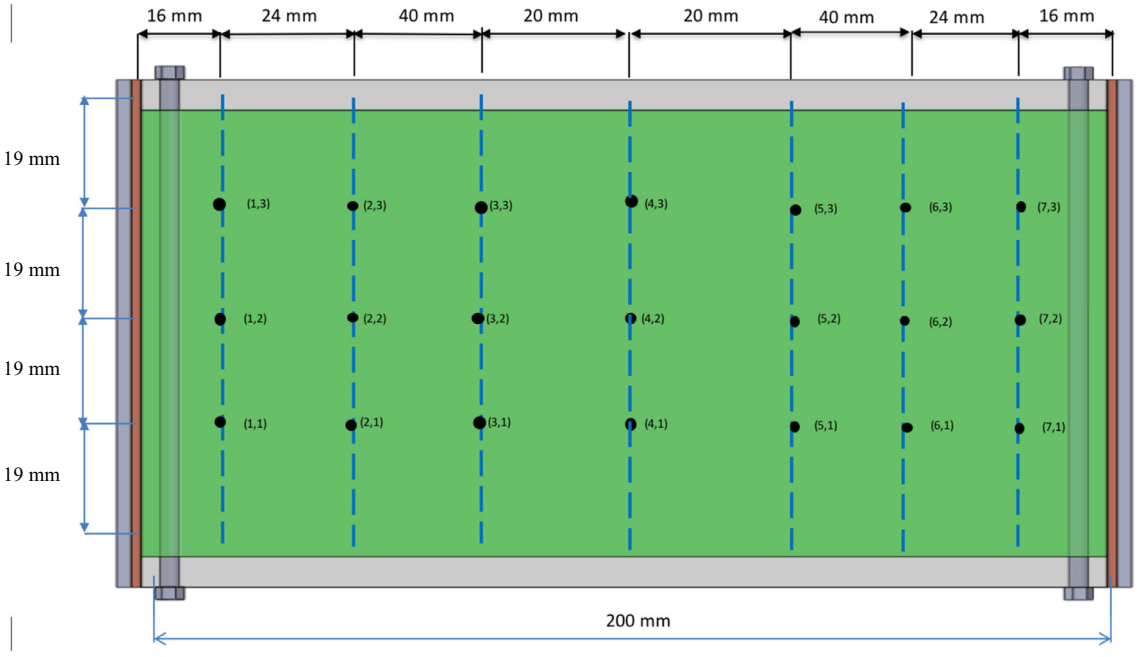

Fig. 3. Thermocouple locations in the vertical mid-plane of the PCM test cell.

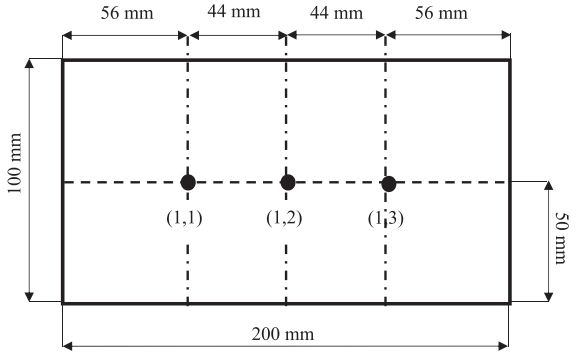

Fig. 4. The location of the three thermocouples installed on the left and right heating surfaces.

The test cell was covered by 100 mm thick thermal insulation (Kingspan Kooltherm [22]) with thermal conductivity of 0.018 W/m K to reduce the heat loss to the surroundings during the experiments. A data acquisition (DAQ) unit, DT85 providing 48 common referenced analogue input channels [23] was used to log the temperature readings. The DAQ unit was connected to a personal computer via a USB port and the dEX software platform was used to configure and manage the logger in real time. The temperatures were recorded at intervals of 10 s for the full duration of the experiment.

In order to record the development and movement of the solid-liquid interface during melting, a Canon 24.2 Megapixel digital camera, Canon EOS 80D [24] with a 18–55 mm lens was used to take photographs every 30 min. A light source behind the store was used to make the solid-liquid interface more visible.

2.1 Experimental test procedure

Before the experiment, the PCM was initially preheated to a temperature of about 40 °C above its melting temperature in an oven before being introduced into the test cell gradually in a layer by layer manner, with each layer allowed to solidify for at least 120 min prior to the next being introduced. This process was continued until the test cell was filled totally with PCM. It should be noted that the objective of this filling procedure is to reduce the formation of voids inside the PCM when it solidifies.

After filling the test cell was kept at room temperature (20 °C to 22 °C) for at least 24 h to ensure that it was at a uniform initial temperature, at this time, the temperature difference between thermocouple measurements was less than 0.1 °C.

3. Experimental data reduction

3.1 Absorbed energy

To determine the amount of energy absorbed by the PCM, both sensible and latent heats were calculated at every data acquisition period. Total sensible heat gain for the liquid and solid regions were calculated by using the following equations [25]:

$$Q_{sensible,PCM}(t) = \int_{V_{liq}(t)} \rho_s C_s (T_{m1} - T_i) dV_{liq} + \int_{V_{liq}(t)} \rho_{liq} C_{liq} \left(T_{mean_{liq}}(t) - T_{m2}\right) dV_{liq} + \int_{V_s(t)} \rho_s C_s (T_{mean_s} - T_i) dV_s \quad (1)$$

where $T_{\mathrm{mean}_{liq}}(t)$ and $T_{\mathrm{mean}_s}(t)$ represent the instantaneous mean temperatures of liquid and solid phases, respectively which were calculated by averaging the temperatures of thermocouples located in each region as follow:

$$T_{\mathrm{mean}_{liq}}(t) = \frac{1}{n_l(t)} \sum_{i=1}^{n_{liq}(t)} T_i \quad (2)$$

$$T_{\mathrm{mean}_s}(t) = \frac{1}{n_s(t)} \sum_{i=1}^{n_s(t)} T_i \quad (3)$$

where $n_{liq}(t)$ and $n_s(t)$ represent the number of thermocouples located in each of the liquid and solid regions of the PCM at each measurements time, respectively.

The latent heat of the region related to the thermocouple is calculated using the equation:

$$Q_{Latent,PCM}(t) = f M_{PCM} h_{latent} \quad (4)$$

where f is the value of the liquid fraction percentage.

The total absorbed energy by the PCM for each thermocouple region is then given by the sum of the latent and sensible heats which have been estimated by Eqs. (1) and (4).

$$Q_{total,PCM}(t) = Q_{sensible,PCM}(t) + Q_{latent,PCM}(t) \quad (5)$$

Newton's law of cooling can be used to evaluate the surface-averaged natural convective heat transfer coefficient during melting.

$$h(t) = \frac{Q_{total,PCM}(t)}{A_w (T_w - T_m) \Delta t} \quad (6)$$

where $Q_{total,PCM}(t)$ is the total heat transfer from the hot walls to the PCM during the time interval (Δt). A_w is the total surface area over which the heat flux is provided. T_w is the average heated wall temperature and T_m is the solid-liquid interface temperature which was considered to be the melting temperature of the PCM.

The characteristic length is calculated using Eq. (7):

$$H = \frac{L \times W}{2(L + w)} \quad (7)$$

where W is the width of the heating plate and L is the height.

The dimensionless average Nusselt number, based on the characteristic length of the test cell (height H) can be written as:

$$\bar{Nu}_{(t)} = \frac{\bar{h}_{(t)} H}{K_{liq}} \quad (8)$$

Table 1
Non-dimensional numbers.

Run No.	q''	Ra ($x10^7$)	Ste
1	675	6.2	1.02
2	960	8.8	1.45
3	1295	11.9	1.95

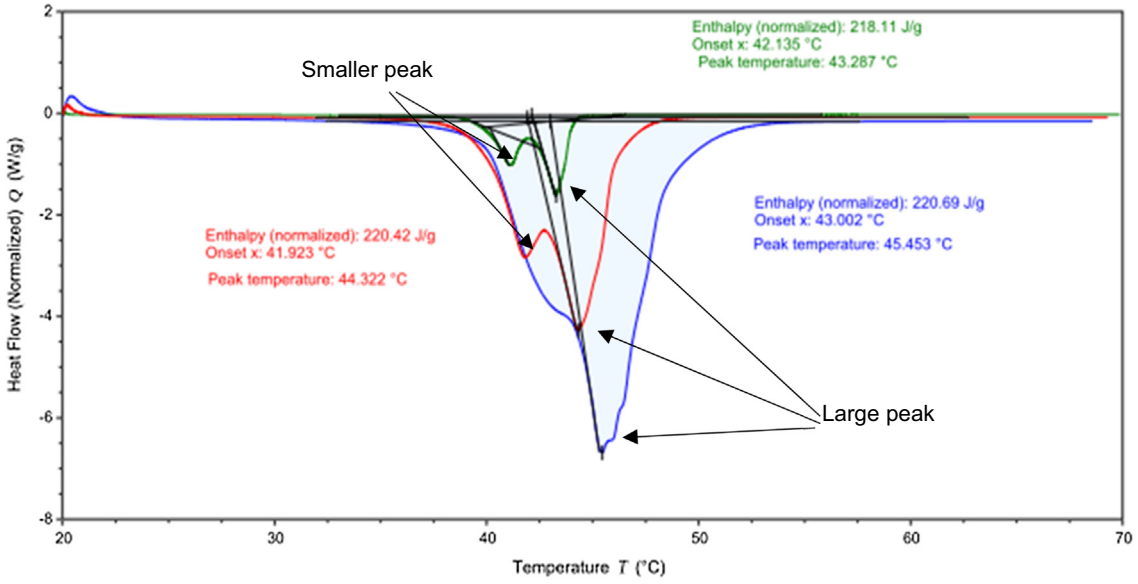

Fig. 5. The melting curve of RT44HC obtained using Differential Scanning Calorimetry.

The relevant dimensionless numbers of the described physical problem are the Stefan number *Ste* and Rayleigh number:

$$Ste = \frac{C_{p,l}\, q'' H}{K\ h_{latent}}, \quad Ra \frac{\rho_l^2 Cp_l g \beta H^4\, q''}{\mu\ K} \tag{9}$$

The aforementioned dimensionless numbers for each of the experiments performed are listed in Table 1.

3.2. Input power

Using the measured voltage and current supplied to the heaters during the experiments, the typical input power supplied to the PCM was calculated, and determined to be 27, 38.4 and 51.8 Watts. The constant wall heat flux, q'' to the system was calculated based on the electric power dissipated over the heat transfer surface area and is given in Eq. (10):

$$q'' = \frac{I\ V}{A_w} = \frac{IV}{2\ L\ w} \tag{10}$$

where A_w is the total surface area of both heaters providing the heat flux to the system.

Table 2
Thermophysical properties of paraffin wax RT44HC.

Thermal conductivity (k_s)	0.2 W/m K
Thermal conductivity (k_{liq})	0.2 W/m K
Specific heat of solid phase $(C_p)_s$	2000 J/kg K
Specific heat of liquid phase $(C_p)_{liq}$	2000 J/kg K
Density: solid phase (ρ_s)	800 kg/m^3
Density: liquid phase (ρ_{liq})	700 kg/m^3
Volumetric expansion coefficient (β)	0.00259 K^{-1}
Dynamic viscosity (μ_{liq})	0.008 kg/m s

3.3 Thermophysical properties of the PCM used

RT44HC a commercially available material (Rubitherm GmbH-Germany) [26] was used because it has a high latent heat of fusion, is chemically stable, does not degrade over multiple cycles, is non-corrosive, and non-toxic. This material has a high heat storage capacity over a narrow temperature range which makes it suitable for solar energy applications, domestic hot water and space heating.

In order to determine the specific heat capacity of the PCM during the melting process, measurements were performed using a TA Instruments Differential Scanning Calorimeter (DSC) [27] with an average error less than 1.0% and a liquid nitrogen cooling system. The measurements were performed with heating/cooling rates of 1 °C.min^{-1}, 5 °C.min^{-1} and 10 °C.min^{-1} and a temperature range from 20 to 70 °C. The measured temperature enthalpy curve recorded during the melting process for RT44HC is shown in Fig. 5.

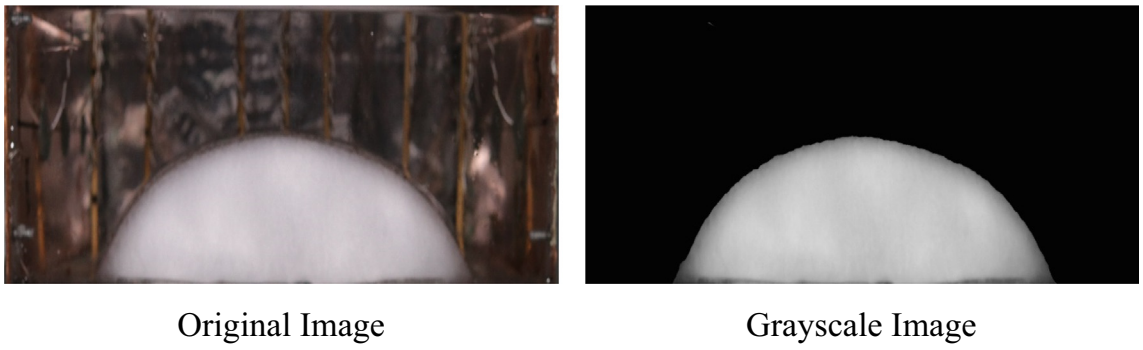

Fig. 6. An initial and processed image to identify the solid-liquid interface, white is solid PCM, black is liquid PCM.

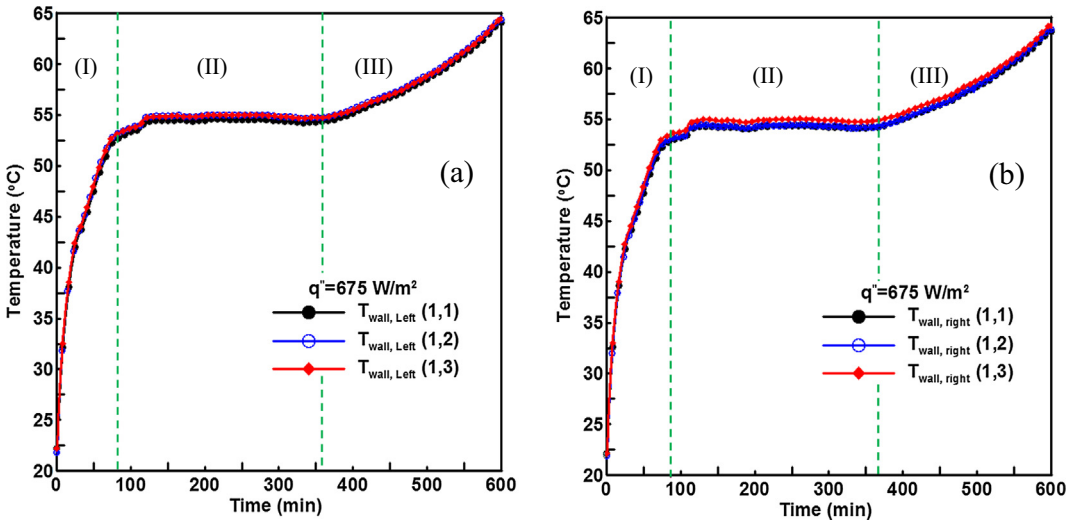

Fig. 7. Measured heated wall surface temperatures in the vertical direction for a heat flux, $q'' = 675$ W/m^2, (a) Left wall. (b) Right wall. (I) Conduction Phase (II) Transient Convection Phase and (III) Quasi-Steady Convection Phase.

The measurements indicate that the melting temperature range of RT44HC is within 42.13–43.28 °C, and the latent heat is 218110 J/kg. The other thermophysical properties of RT44HC were adopted from [28] (see Table 2).

4. Melt front evolution

To evaluate the melt fraction and the location of the moving solid-liquid interface, the insulation of the front face of the test cell was periodically removed and a colour digital image was taken every 30 min. The image was converted to a black and white image which consists of a two-dimensional array with either zero or one in each cell corresponding to black and white pixels respectively. The MATLAB image processing toolbox [29] was utilized to determine the instantaneous liquid fraction based on the number of zeros and ones in the array. Fig. 6 shows the steps used for calculating the liquid fraction.

The liquid fraction was evaluated by dividing the number of zeros in the array by the total number of pixels forming the image.

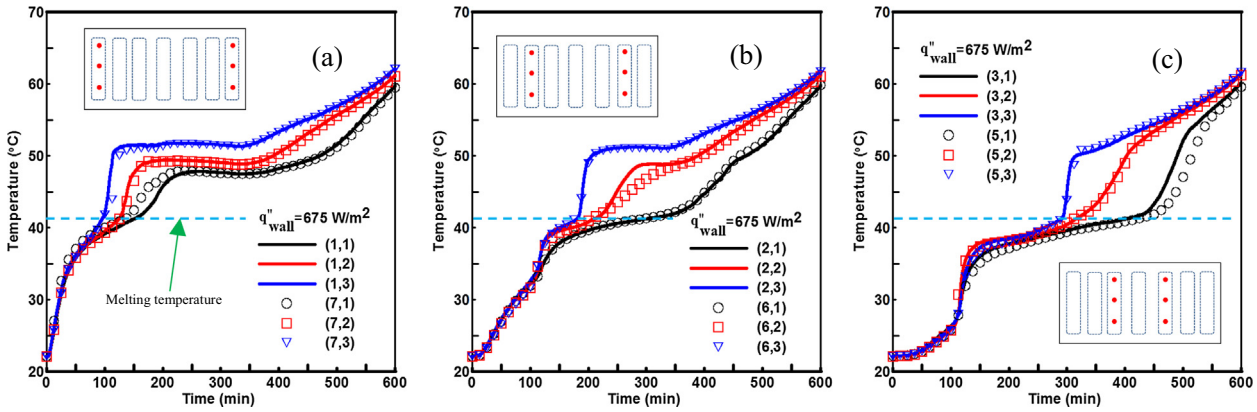

Fig. 8. Measured temperatures at the 18 thermocouple locations within the test cell with time for a wall heat flux of q″ = 675 W/m^2.

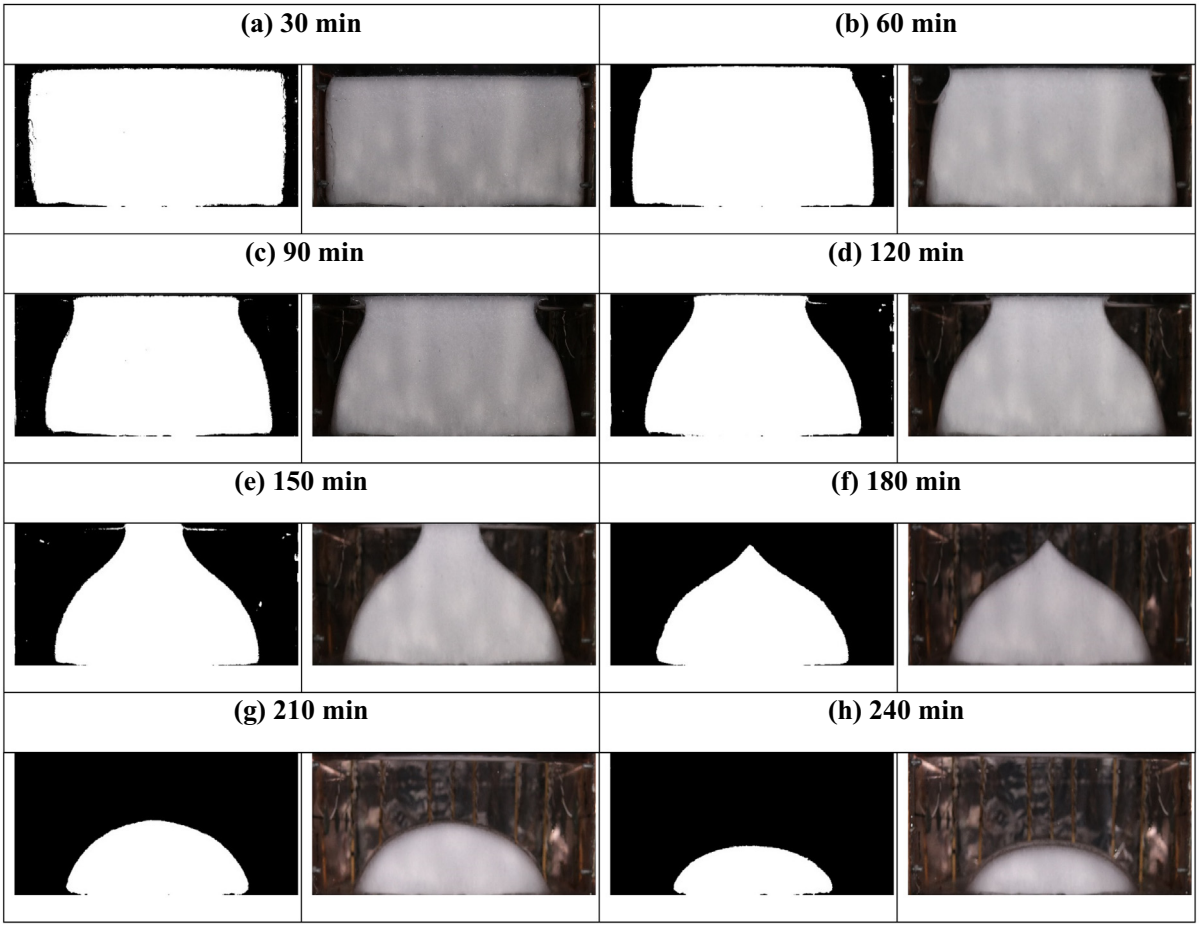

Fig. 9. Pictures illustrating the melting front progression in the rectangular test cell filled with RT44HC for wall heat flux of q″ = 1295 W/m^2 at both vertical walls. Black regions represent liquid PCM and white regions solid.

$$f = \frac{NP_0}{NP_t} \tag{11}$$

where NP_0 and NP_t are the number of 0 values in the array and total number of cells in the array, respectively.

5. Experimental results and discussion

To confirm the performance of the developed experimental setup with heating from two sides, initial experiments were performed to check that melting occurred symmetrically. Fig. 7 presents the temperatures measured by the thermocouples on the heated wall with time for a constant heat input of 27 W (corresponding to a heat flux of 675 W/m^2) applied to the left and right sides of the enclosure. For all locations on each side, similar temperatures were recorded confirming the symmetrical heat input. In the early stage of heating and the initial PCM melting phase (<80 min) the heat transfer is conduction dominated in the PCM and the heated surface temperatures in the vertical direction are similar and show a nearly linear increase with time **(Conduction Phase (I))**. After 80 min, the liquid PCM layer adjacent to the heated walls increases in thickness and natural convection starts to drive the hot liquid PCM upwards due to the density difference between the hotter and cooler liquid PCM, the temperature of the hot wall remains almost constant because of onset of natural convection in the liquid PCM **(Transient Convection Phase (II))**. As melting progress (t > 360 min) the fluid circulation continues to grow increasing the melt fraction. Natural convection becomes dominant and the heat transfer coefficient from the heated surface to the PCM increases meaning that the power input is transferred from the wall to the PCM for a smaller temperature difference, therefore, the rate of increase of local wall surface temperature slows down **(Quasi-Steady Convection Phase (III)).**

The temperatures measured with the thermocouples inside the test cell are presented in Fig. 8 for a heat flux q″ = 675 W/m^2. During the early stages of the experiment, the thermocouples mounted

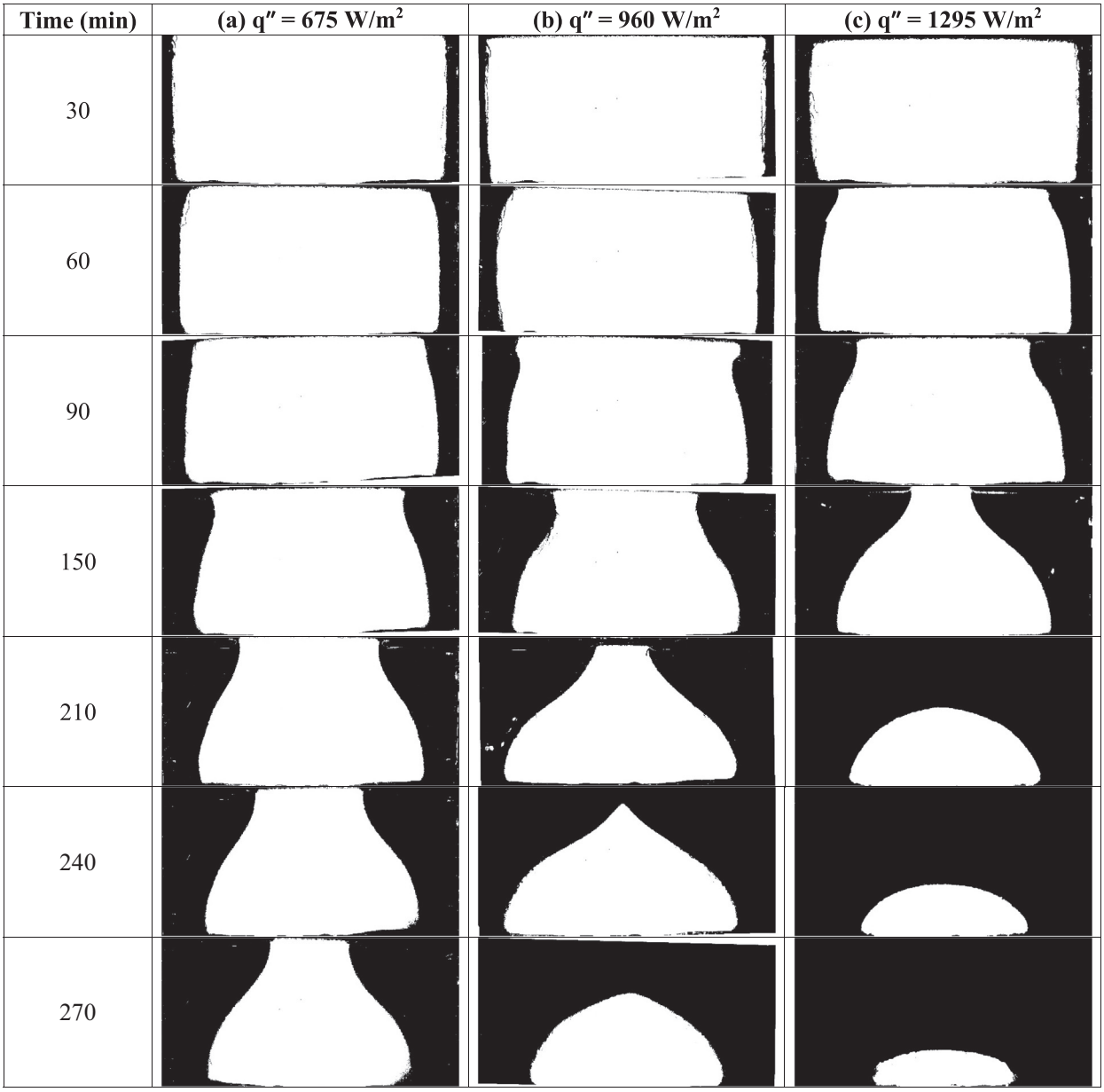

Fig. 10. A sequence of photographs showing melt front progression with time for three wall heat fluxes, (a) q″wall = 675 W/m^2, (b) q″wall = 960 W/m^2 and (c) q″wall = 1295 W/m^2.

on the first column (Fig. 8a) show a higher temperature increase than those of the second and third columns (Fig. 8b) and (Fig. 8c) which shows conduction heat transfer in the solid.

Fig. 8(a) shows that when the PCM melting temperature is achieved the rate of temperature increase in the first column of thermocouples is much higher than those of second and third columns (Fig. 8b and c). This can be explained by the fact that the heat transfer to the solid PCM surrounding the first column of thermocouples is high due to convection in the melt and heat conduction through a thin layer of solid PCM surrounding the thermocouples.

From Fig. 8, it can be seen that when the PCM adjacent to the heated walls is molten, convection develops and the temperatures in the upper part of the enclosure are generally higher than the temperatures in the lower part. Also, a rapid increase in temperature can be seen in the temperature distributions which occurs when the melt front is passing between two adjacent thermocouples. This can be used for estimation of the melt front location based on each thermocouple's location. The convection currents in the liquid PCM adjacent to the left and right heated walls result due to the increase in PCM temperature due to the constant rate heat input. The heated less dense liquid rises up the wall and is deflected at the test cell top surface prior to flowing down the solid-liquid interface in the PCM. The left side flow is in the clockwise direction and the right-side flow is anticlockwise maintaining symmetry. At the solid-liquid interface, heat is transferred from the warm liquid to the cooler solid PCM (causing it to melt) and cooling the liquid which becomes more dense and sinks.

6. Solid-liquid interface tracking

Fig. 9 presents photographs taken every 30 min during the experiment (with a uniform wall heat flux of $q'' = 1295\ W/m^2$ imposed on the left and right walls) showing the progress of the solid-liquid interface during the melting of RT44HC.

In these photographs, white and black areas represent the solid and liquid phases, respectively. The symmetrical nature of the melting process can be clearly seen. From Fig. 9 the melting process can be characterized into four distinct regimes (i) conduction dominated melting [30 min], (ii) mixed convection-conduction melting [60–90 min], (iii) convection dominated melting prior to left and right-side flows meeting [120–1500 min], (iv) convection dominated melting after left and right-side flows have met [180–240 min].

Up to 30 min the solid-liquid interface was almost vertical parallel to the heated plate due to heat transfer being predominantly by conduction. This mode of heat transfer prevailed while the viscous force was sufficient to suppress fluid motion (Fig. 9a). With the elapse of time, more RT44HC is heated and melts, the buoyancy force resulting from the increased temperature and reduction in density becomes sufficient to overcome the viscous force and natural convection occurs in the liquid region. The resulting convective flow leads to an increase in melting at the top of the container and an acceleration in the movement of the solid-liquid interface in this region compared to lower down on the heated wall. The flow changed direction at the top of the container impinging on the solid PCM and creating a concave curve at the top of the melt front seen in Fig. 9(b and c). As the melting progresses, natural convection intensifies and its effect on the melt front becomes more pronounced. The increasing curvature of the melt front in the upper part of the enclosure provides evidence of this effect.

The rapid change in the melt layer thickness at the top results from the flow changing direction and the hot fluid flowing along the underside of the top surface and impinging on the solid PCM at the top of the container. In the lower part of the enclosure, the shape of the interface remains almost linear, its angle of inclination increases as the solid PCM shrinks. This pattern of melting continues until the solid PCM melts completely.

Fig. 10 shows the melt front shapes at different times for the three-wall heat flux values $q''_{wall} = 1295\ W/m^2$, $q''_{wall} = 960\ W/m^2$ and $q''_{wall} = 675\ W/m^2$. As expected, melt front evolution is nearly symmetrical with similar profiles produced when different wall fluxes are imposed on both left and right walls. It can be seen that the melt front advances faster when the wall heat flux is increased.

From Fig. 11 it can be seen that as the wall flux increases, the time for total melting decreases, this is expected due to the increased rate of heat transfer to the enclosure. The increase in power input also led to an increase in the average temperature

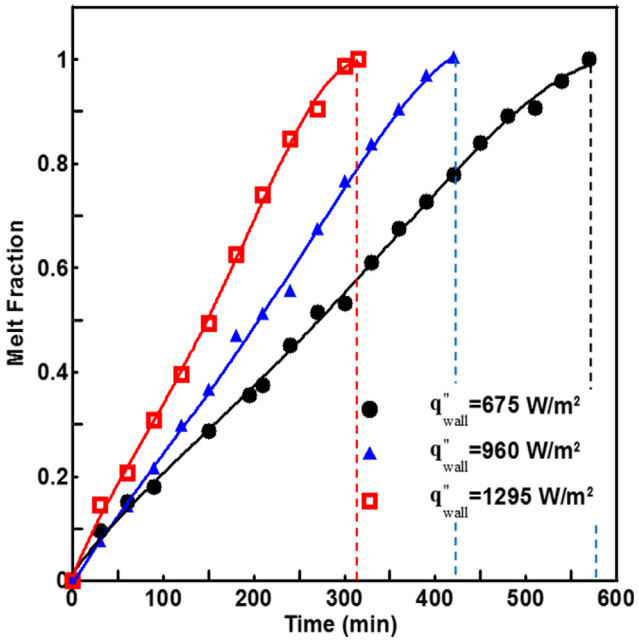

Fig. 11. Melt fraction versus time for three different wall heat fluxes.

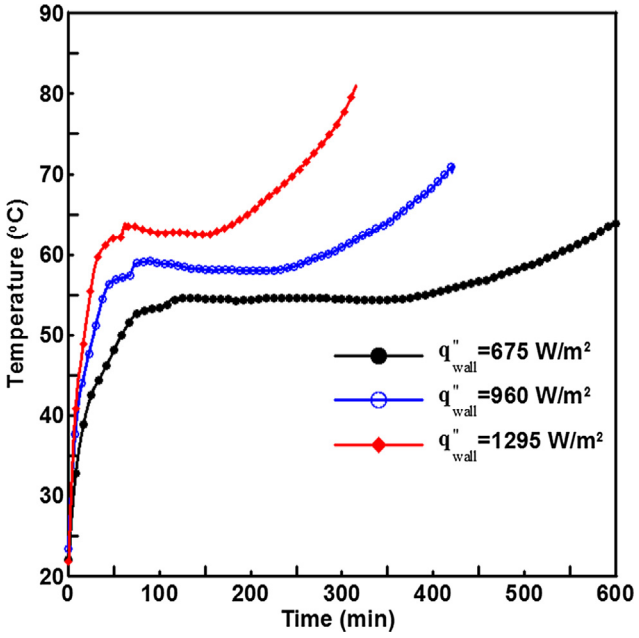

Fig. 12. The temperature history along the hot wall for three different wall heat fluxes.

of both the PCM and the heating surface. Increasing the input power from 675 W/m^2 to 960 W/m^2 to 1295 W/m^2 reduces the total time for the melting process by 26.3% and 42.10% respectively.

The hot wall temperature was evaluated by averaging thermocouple measurements along the vertical centre line of the copper wall. Fig. 12 shows the temperature history along the hot wall at the three constant heat flux values. It can be observed from

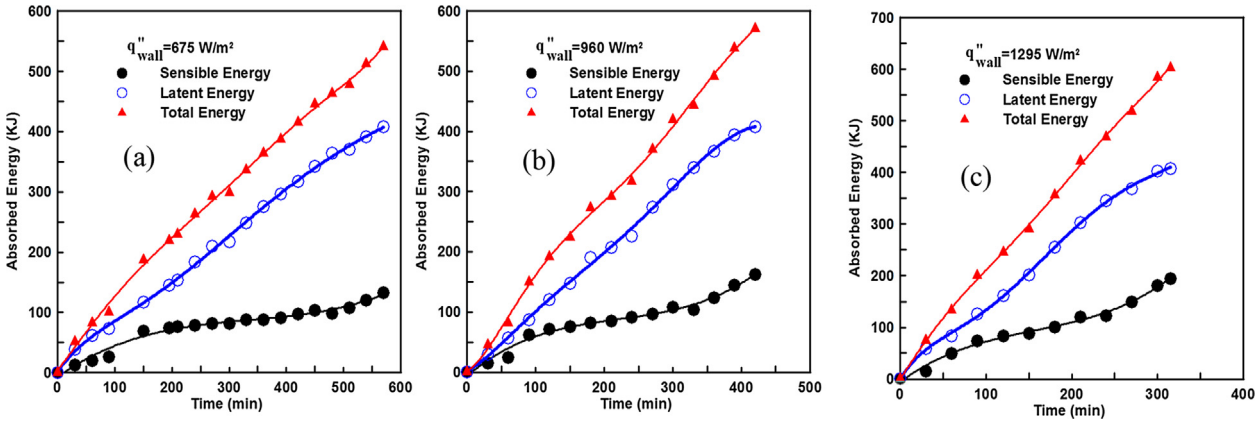

Fig. 13. Calculated sensible heat, latent heat and total heat absorbed with time in the PCM test cell for wall heat flux values of (a) q″ = 675 W/m^2, (b) q″ = 960 W/m^2, and (c) q″ = 1295 W/m^2.

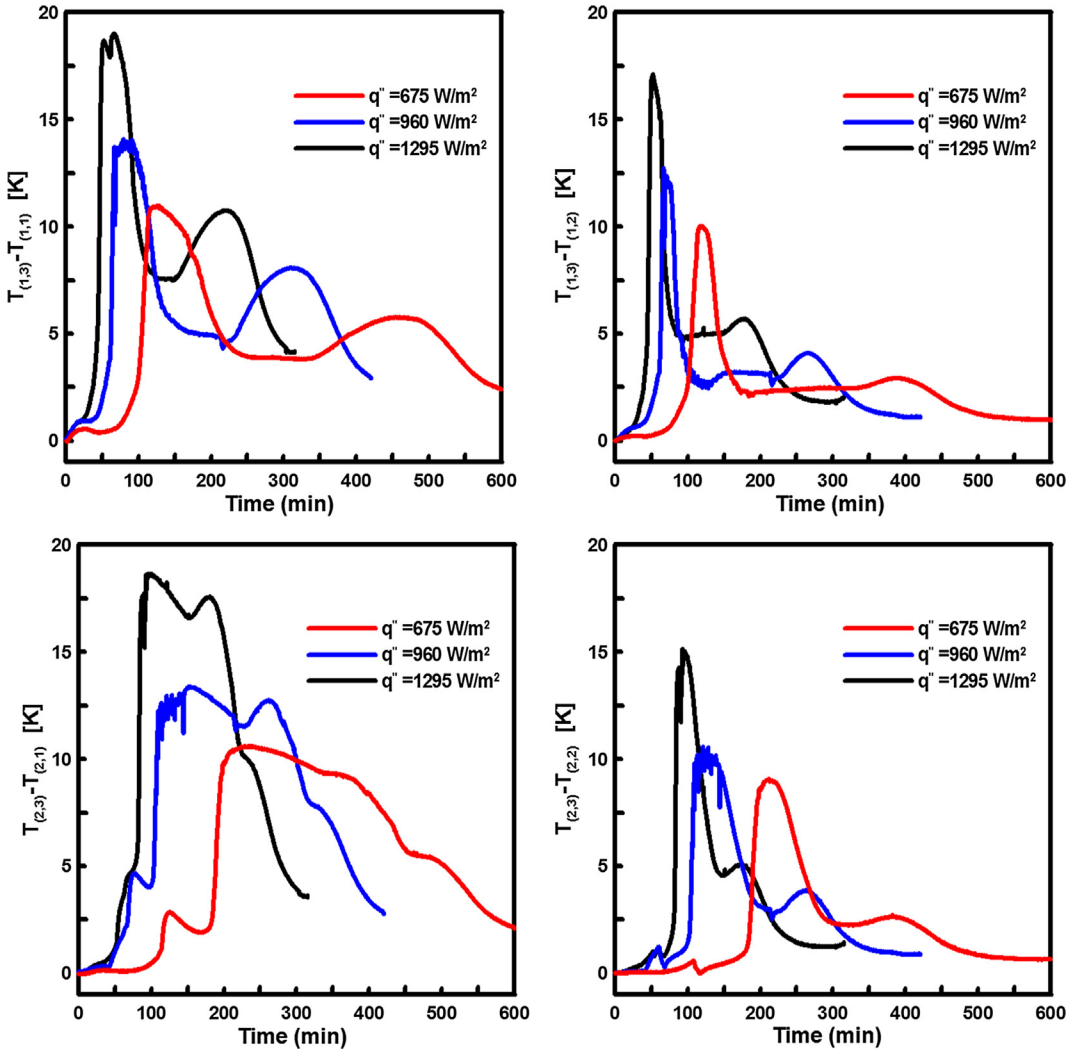

Fig. 14. Variation of the measured temperature difference recorded by thermocouples located at position $T_{(i,3)}$ (top) and $T_{(i,1)}$ (bottom) and $T(i,2)_{(middle)}$ for the three values of wall heat flux q″ = 675, 960 and 1295 W/m^2.

Fig. 12 that the hot wall temperature rises linearly with time following the initial start-up. This shows that melting is determined by conduction in the early stages. The conduction dominated period lasts for 50 min, 75 min and 100 min for heat fluxes of 1295, 960 and 675 W/m^2, respectively. The wall temperatures rise to 63 °C, 57 °C and 53 °C during conduction dominated phases. Afterwards, the temperature of the hot wall remains almost constant because of the onset of natural convection in the melting PCM. As time progresses, the temperature of the hot wall starts to increase slowly until the end of the melting process.

Fig. 13 shows the calculated increase in sensible, latent and total stored energy within the test cell at every 30 min for different wall heat flux values. As can be seen in Fig. 13, the contribution of latent heat to the total heat absorbed is much greater than sensible heat. As expected for all values of wall heat flux, the maximum values of absorbed latent heat are equal since they are a function of the test cell volume which is constant for all experiments. It can be observed that the values of the maximum total energy absorbed change slightly due to the change of hot wall temperature which is the result of different values of heat flux.

Fig. 14 presents the differences in temperature recorded by thermocouples located in positions $T_{(i,3)}$ (top of the vertical mid-plane of the enclosure) and $T_{(i,1)}$ (bottom of the vertical mid-plane of the enclosure) and $T_{(i,2)}$ (middle of vertical mid-plane of the enclosure) for the three values of wall heat flux.

In the first 50 min, the rise in the measured temperature differences are similar for all flux values due to conduction in the solid PCM being the main heat transfer mechanism. At t = 50 min, the thermocouples in the upper locations show a much greater temperature rise than those in the middle and bottom locations due to the onset of natural convection in the liquid PCM which increases the local heat transfer rate between the solid and liquid PCM in the upper section of the enclosure. The value of the increase in temperature difference is an indicator of the strength of the local heat transfer rate at the solid-liquid interface. The higher values of wall heat flux increase the rate at which the temperature difference is established suggesting a faster onset of convection and a higher rate of convection at higher wall heat fluxes. When the RT44HC melted fully, natural convection increased mixing in the liquid RT44HC, leading to the gradual decrease in the temperature difference observed.

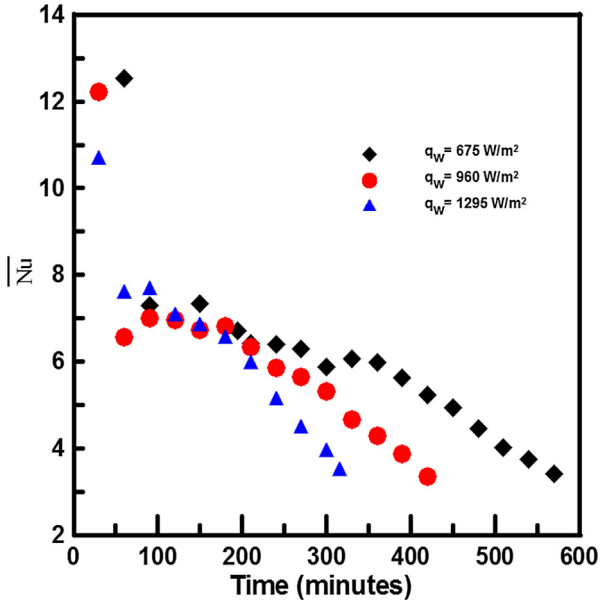

Fig. 15. Variation of the Nusselt number with wall heat flux.

The variation of Nusselt number with time for the three wall heat flux values is presented in Fig. 15. The variation of the Nusselt number shows the strength of the convective heat transfer during the melting process. In each experiment, the Nusselt number starts with a relatively high value at the initiation of the heat transfer process and drops very rapidly during the conduction regime. The initial Nusselt number is attributed to the small thermal resistance of the very thin liquid layer at the start-up of the experiments which accordingly increases the magnitude of Nusselt number.

At the end of the conduction regime, the Nusselt number experiences a local minimum value and then increases slightly. This local increase in Nusselt number shows that natural convection is initiating, and the heat transfer process is now in transition and includes both conduction and convection.

As the experiment proceeds, the length of the solid-liquid boundary reduces and the Nusselt number reduces for the remainder of the melting process. The decrease in the Nusselt number towards the end of the experiments is due to a reduction in convective heat transfer due to the reduction in the length of the melting front [5].

7. Conclusions

In the current study, an experimental investigation was conducted to explore the melting of PCM RT44HC in a horizontally oriented rectangular cross-section test cell to examine the effect of different values of wall heat on the development of the melt fraction, PCM average temperature, amount of absorbed energy, temperature distributions, wall heater surface temperature and the Nusselt number. Images of the melting process and the instantaneous temperature distribution at the vertical mid-plane of the enclosure are presented. The images of the melting process were analysed using an image processing technique to measure the melt fraction development with time. The development of the melt front and recorded temperature distributions were employed to analyse the dominant mode of heat transfer during the different stages of melting. Based on the finding it is concluded that

- At higher values of wall heat flux, the average temperature of the heater's surface and the PCM increased and the total melting time reduced.
- Conduction is the dominant mode of heat transfer during the early stage of melting which is followed by a short transition period before convection dominates the remainder of the melting process.
- Increasing the input power from 675 W/m^2 to 960 W/m^2 to 1295 W/m^2 reduces the total time for the melting process by 26.3% and 42.10% respectively.
- The experimental measurements provide a set of benchmark data suitable to verify numerical models of PCM melting in rectangular containers.

Declaration of Competing Interest

The authors declare no conflicts of interest.

Acknowledgements

The authors are grateful to the Engineering and Physical Sciences Research Council (EPSRC) for funding this work through Grant reference EP/N021304/1 and EP/K011847/1.

Appendix

Analysis of experimental uncertainty

To estimate the uncertainty in the results. The uncertainties in the primary measurements were required. The experimental uncertainty analysis was then performed based on the methods described in [30]. Assuming that the final results are derived from independent variables y_1, $y_2 \ldots, y_n$. The uncertainty of result W is obtained by appropriately combining the uncertainty of the independent variables $W(y_i)$ as fellow:

$$K = f(y_1, y_2, \cdots, y_n) \tag{12}$$

$$W(K) = \sqrt{\sum_{i=1}^{n} \left(\frac{\partial f}{\partial y} W(y_i)\right)^2} \tag{13}$$

By applying this method, the maximum uncertainties of melt fractions and Nusselt number were found to be 3.8% and 7.5%, respectively.

Appendix A. Supplementary material

Supplementary data to this article can be found online at https://doi.org/10.1016/j.ijheatmasstransfer.2019.06.047.

References

[1] M.S. Al-Jethelah, S.H. Tasnim, S. Mahmud, A. Dutta, Melting of nano-phase change material inside a porous enclosure, Int. J. Heat Mass Transf. 102 (2016) 773–787, https://doi.org/10.1016/j.ijheatmasstransfer.2016.06.070.

[2] S. Almsater, Alemu Alemu, W. Saman, F. Bruno, Development and experimental validation of a CFD model for PCM in a vertical triplex tube heat exchanger, Appl. Therm. Eng. 116 (2017) 344–354, https://doi.org/10.1016/j.applthermaleng.2017.01.104.

[3] M.D. Muhammad, O. Badr, H. Yeung, Validation of a CFD melting and solidification model for phase change in vertical cylinders, Numer Heat Transf Part A Appl 68 (2015) 501–511, https://doi.org/10.1080/10407782.2014.994432.

[4] M.J. Huang, P.C. Eames, B. Norton, Thermal regulation of building-integrated photovoltaics using phase change materials, Int. J. Heat Mass Transf. 47 (2004) 2715–2733, https://doi.org/10.1016/j.ijheatmasstransfer.2003.11.015.

[5] M.H. Joneidi, M.J. Hosseini, A.A. Ranjbar, R. Bahrampoury, Experimental investigation of phase change in a cavity for varying heat flux and inclination angles, Exp. Therm. Fluid Sci. 88 (2017) 594–607, https://doi.org/10.1016/j.expthermflusci.2017.07.017.

[6] F. Agyenim, N. Hewitt, P. Eames, M. Smyth, A review of materials, heat transfer and phase change problem formulation for latent heat thermal energy storage systems (LHTESS), Renew. Sustain. Energy Rev. 14 (2010) 615–628, https://doi.org/10.1016/j.rser.2009.10.015.

[7] N.S. Dhaidan, J.M. Khodadadi, Melting and convection of phase change materials in different shape containers: a review, Renew. Sustain. Energy Rev. 43 (2015) 44977, https://doi.org/10.1016/j.rser.2014.11.017.

[8] M. Fadl, P. Eames, A numerical investigation into the heat transfer and melting process of lauric acid in a rectangular enclosure with three values of wall heat flux, Energy Procedia 158 (2019) 4502–4509, https://doi.org/10.1016/J.EGYPRO.2019.01.761.

[9] Y. Wang, A. Amiri, K. Vafai, An experimental investigation of the melting process in a rectangular enclosure, Int. J. Heat Mass Transf. 42 (1999) 3659–3672, https://doi.org/10.1016/S0017-9310(99)00024-1.

[10] H. El Qarnia, A. Draoui, E.K. Lakhal, Computation of melting with natural convection inside a rectangular enclosure heated by discrete protruding heat sources, Appl. Math. Model 37 (2013) 3968–3981, https://doi.org/10.1016/J.APM.2012.08.021.

[11] Z.-X. Gong, S. Devahastin, A.S. Mujumdar, Enhanced heat transfer in free convection-dominated melting in a rectangular cavity with an isothermal vertical wall, Appl. Therm. Eng. 19 (1999) 1237–1251, https://doi.org/10.1016/S1359-4311(99)00003-4.

[12] J. Zhao, J. Zhai, Y. Lu, N. Liu, Theory and experiment of contact melting of phase change materials in a rectangular cavity at different tilt angles, Int. J. Heat Mass Transf. 120 (2018) 241–249, https://doi.org/10.1016/j.ijheatmasstransfer.2017.12.006.

[13] B. Kamkari, H. Shokouhmand, F. Bruno, Experimental investigation of the effect of inclination angle on convection-driven melting of phase change material in a rectangular enclosure, Int. J. Heat Mass Transf. 72 (2014) 186–200, https://doi.org/10.1016/j.ijheatmasstransfer.2014.01.014.

[14] M.J. Huang, P.C. Eames, B. Norton, N.J. Hewitt, Natural convection in an internally finned phase change material heat sink for the thermal management of photovoltaics, Sol. Energy Mater. Sol. Cells 95 (2011) 1598–1603, https://doi.org/10.1016/j.solmat.2011.01.008.

[15] B. Kamkari, H.J. Amlashi, Numerical simulation and experimental verification of constrained melting of phase change material in inclined rectangular enclosures, Int. Commun. Heat Mass Transf. 88 (2017) 211–219, https://doi.org/10.1016/j.icheatmasstransfer.2017.07.023.

[16] M. Emam, S. Ookawara, M. Ahmed, Thermal management of electronic devices and concentrator photovoltaic systems using phase change material heat sinks: experimental investigations, Renew. Energy 141 (2019) 322–339, https://doi.org/10.1016/J.RENENE.2019.03.151.

[17] V. Shatikian, G. Ziskind, R. Letan, Numerical investigation of a PCM-based heat sink with internal fins, Int. J. Heat Mass Transf. 48 (2005) 3689–3706, https://doi.org/10.1016/j.ijheatmasstransfer.2004.10.042.

[18] B. Kamkari, H. Shokouhmand, Experimental investigation of phase change material melting in rectangular enclosures with horizontal partial fins, Int. J. Heat Mass Transf. 78 (2014) 839–851, https://doi.org/10.1016/j.ijheatmasstransfer.2014.07.056.

[19] Z. Huang, N. Xie, X. Zheng, X. Gao, X. Fang, Y. Fang, et al., Experimental and numerical study on thermal performance of Wood's alloy/expanded graphite composite phase change material for temperature control of electronic devices, Int. J. Therm. Sci. 135 (2019) 375–385, https://doi.org/10.1016/J.IJTHERMALSCI.2018.09.031.

[20] H. Usman, H.M. Ali, A. Arshad, M.J. Ashraf, S. Khushnood, M.M. Janjua, et al., An experimental study of PCM based finned and un-finned heat sinks for passive cooling of electronics, Heat Mass Transf. Und Stoffuebertragung 54 (2018) 3587–3598, https://doi.org/10.1007/s00231-018-2389-0.

[21] Copper Sheet. (accessed February 21, 2018). <https://www.themetalstore.co.uk>.

[22] Kingspan Kooltherm. (accessed February 2, 2018). <https://www.insulationsuperstore.co.uk>.

[23] dataTaker Intelligent Data Loggers DT85. (accessed February 2, 2018). <http://www.datataker.com/>

[24] Canon. Canon EOS 1100D. (accessed February 21, 2018). <https://www.canon.co.uk/>.

[25] H. Shokouhmand, B. Kamkari, Experimental investigation on melting heat transfer characteristics of lauric acid in a rectangular thermal storage unit, Exp. Therm. Fluid Sci. 50 (2013) 201–222, https://doi.org/10.1016/j.expthermflusci.2013.06.010.

[26] Rubitherm GmbH. 2014. (accessed February 21, 2018). <https://www.rubitherm.eu/>.

[27] TA Instruments User Training.

[28] J. Pereira, D. Cunha, P. Eames, Compact latent heat storage decarbonisation potential for domestic hot water and space heating applications in the UK, Appl. Therm. Eng. (2018), https://doi.org/10.1016/j.applthermaleng.2018.01.120.

[29] Image Processing Toolbox. (accessed February 21, 2018). <https://uk.mathworks.com>.

[30] R.J. Moffat, Describing the uncertainties in experimental results, Exp. Therm. Fluid Sci. 1 (1988) 3–17, https://doi.org/10.1016/0894-1777(88)90043-X.